JMEPEG (2019) 28:7097–7108
https://doi.org/10.1007/s11665-019-04438-9

1059-9495/$19.00

Tensile Properties of a Cast Al-Si-Mg Alloy with Reduced Si Content and Cr Addition at High Temperature

Marialaura Tocci, Riccardo Donnini, Giuliano Angella, Elisabetta Gariboldi, and Annalisa Pola

(Submitted May 28, 2019; in revised form October 25, 2019; published online November 7, 2019)

Tensile properties of an Al-Si-Mg casting alloy with reduced Si content and Cr addition were investigated at room and high temperatures. It was found that the studied alloy exhibits a remarkable performance up to 200 °C, with comparable or slightly higher strength than typical values for Al-Si-Mg-Cu alloys, commonly used for high-temperature applications, and good elongation. This is due to the choice of proper heat treatment and to the formation of dispersoids containing Cr during heat treatment, which are stable at the considered temperatures, as demonstrated by scanning and transmission electron microscopy (STEM) analysis. Interestingly, exposure to 300 °C during tensile tests enhanced an additional formation of dispersoids. It is believed that heating the material in T6 condition led to such observed dispersoids formation since precursors were already present in the Al matrix. This is not sufficient to avoid material softening at 300 °C, but it represents an interesting point in order to develop alternative heat treatment routes for dispersion-strengthened Al alloys.

Keywords Al alloys, dispersion strengthening, heat treatment, mechanical properties, microstructure, precipitation strengthening

1. Introduction

Al-Si-Mg alloys castings are known to exhibit remarkable mechanical properties at room temperature, while they suffer from overaging when exposed to high temperatures. This is a serious limitation to their application, and it is particularly relevant for the transport field, where these alloys are widely used to replace steel components. In fact, weight reduction of vehicles is a key issue in order to meet the strict limits for toxic emissions in atmosphere. On the other hand, for certain applications in the automotive field, the components operate at temperature well above room condition, as, for instance, cylinder heads, manifolds, heat exchangers, internal combustion engine pistons and crankcases, which can be exposed up to 300 °C (Ref 1).

In this regard, the addition of alloying elements in order to improve the performance of Al-Si-Mg alloys for high-temperature applications is widely studied in the scientific literature. For instance, the addition of Cu enhances the thermal stability of the material due to the formation of Cu-based precipitates during aging treatment (Ref 2-4). These are more thermally resistant than Mg-containing ones, even though prolonged exposure can lead to their coarsening and, consequently, to a general material softening (Ref 5). Al-Si-Cu-Mg alloys are typically used for the production of engine components (Ref 6-8), which can be exposed to high-temperature conditions. However, the presence of Cu is known to reduce the corrosion resistance (Ref 9) and, therefore, it could be critical for applications in aggressive environments. Therefore, new alloys compositions, aiming at the improvement of the performance at high temperature, are still under investigation. For instance, the addition of transition metals such as Zr, Ti and V to cast alloys was also analyzed by different authors and the formation of precipitates containing these elements during aging treatment is reported (Ref 10, 11). It was found that these particles promoted material resistance and exhibited stability at high temperature. The same authors evaluated also the further addition of Cr (Ref 12). Similarly, the influence of various transition elements was investigated for an AlSi10 alloy (Ref 13) with positive results in terms of increased strength of the alloy. The addition of small amounts of Ni (or V) to A356 alloy was not able to strongly affect high-temperature tensile properties (Ref 14), while the presence of Ni was found to be negative at room temperature (Ref 15). Also Sc was considered as strengthening elements in order to enhance mechanical properties, but mainly at room temperature (Ref 16, 17).

Furthermore, the addition of alloying elements that can lead to the formation of dispersoids during solution treatment is a valid alternative to enhance the material performances at high temperature. In this regard, Farkoosh et al. (Ref 18) reported the positive effect on high-temperature tensile and creep behavior of dispersoids containing Mo for a modified Al-Si-Mg alloy in comparison with the base material. For the same reasons, the role of Er and/or Zr has been analyzed in recent studies (Ref 19, 20). The strengthening effect of these elements, if added in the proper amount, was due to the formation of thermally stable Er and Zr-containing dispersoids, as reported also in other studies focused on the microstructure and the mechanical properties of pure Al (Ref 21). In addition, the formation of dispersoids containing Mn and/or Cr is extensively described in the literature (Ref 22, 23), even though the investigations of their

Marialaura Tocci and **Annalisa Pola**, Department of Mechanical and Industrial Engineering, University of Brescia, Via Branze 38, 25123 Brescia, Italy; **Riccardo Donnini** and **Giuliano Angella**, Institute of Condensed Matter Chemistry and Technologies for Energy (ICMATE), National Research Council of Italy (CNR), Via R. Cozzi 53, 20125 Milan, Italy; and **Elisabetta Gariboldi**, Department of Mechanical Engineering, Politecnico di Milano, Via La Masa 1, 20156 Milan, Italy. Contact e-mail: m.tocci@unibs.it.

effect on mechanical properties are more abundant for wrought than for cast alloys.

Lately, an AlSi3Mg alloy containing Cr has been studied. This alloy exhibits remarkable strength and erosion resistance at room temperature (Ref 24, 25) and it is characterized by the formation of dispersoids during solution treatment due to Cr addition (Ref 23). These particles are responsible for enhanced hardness in comparison with the base alloy (Ref 22), but mechanical properties at high temperature have not been investigated to date. This kind of characterization could provide fundamental information to identify new and alternative applications of the studied alloy in the automotive field, for instance, for the above-mentioned components that can be exposed to high temperatures.

Besides the formation of thermally stable precipitates, the reduced Si content of the studied alloy in comparison with the most widely used cast Al-Si alloys represents an alternative solution for the development of non-conventional alloys. In this regard, Si content is reported to significantly affect mechanical properties of Al-Si alloys, enhancing castability, as well as material hardness and strength (Ref 26-28). On the other hand, if the tensile fracture mechanism is considered, eutectic Si particles play a key role in the nucleation and growth of cracks, which usually takes place at the interface between the Al matrix and secondary particles (Ref 29). Si eutectic particles are known to be easily cracked during tensile tests and to represent the main fracture path. In this case, morphology, size, number and distribution of these particles strongly influence material strength and ductility (Ref 29-32).

In the present study, the tensile properties of the AlSi3Mg alloy containing Cr are investigated at room and high temperatures (up to 300 °C). Preliminary tests at room temperature were aimed at optimizing heat treatment parameters, while specimens in a selected heat-treated condition were tested at different temperatures ranging from 150 to 300 °C in order to study the material performance and the thermal stability of dispersoids. Fracture surfaces were observed by electron microscopy to study the fracture mechanism and to correlate it with microstructural features.

2. Experimental Procedure

The chemical composition (in wt.%) of the studied alloy is Si (3-4%), Mg (0.6-0.7%), Cr (0.2-0.3), Fe (< 0.12%), Mn (0.07-0.15%) and Ti (0.10-0.15%), as raw material (ingot) provided by the supplier. Ti is present as refining elements, while no Sr was added as modifier (Ref 33) due to the low Si content.

Samples were produced by low-pressure die casting (LPDC). The alloy was melted in a dry hearth reverberatory furnace. After conventional scorifying operations and chemical composition control, the alloy was moved via a pre-heated ladle to the degassing unit for cleaning operation (performed with nitrogen). Subsequently, the alloy was poured into the holding furnace of the LPDC machine. A LPM machine was used, applying a pressure ramp up to 1.2 bar. The pouring temperature was set to 700 °C, and the furnace was pressurized with a ramp up to 1.2 bar to fill the thermo-regulated permanent mold by forcing the liquid alloy up through the sprue. The pressure was maintained during the solidification of the alloy to counteract shrinkage defects formation. Hence, 19" in. car wheels were produced. Samples were taken from the rim in an area with thickness of 27 mm. Since various microstructural properties (secondary dendrite arms spacing, grain size and eutectic Si particles size and morphology), which are known to affect strength and ductility, are related to the cooling rate, care was taken in producing samples in the same solidification conditions. This allows to guarantee uniform characteristics among the different samples. In particular, in the area of the casting used to obtain the samples for the present study, a solidification rate of 1 °C/s was estimated based on temperature measurements during the cycle by means of thermocouples placed in the mold, in the area of the casting used for producing the specimens.

Samples were tested in as-cast and various T6 (solution, quenching and aging treatment) heat-treated conditions. Samples with size of approximately 20 × 20 × 10 mm^3 were cut from the casting for microstructural characterization and hardness measurements. As-cast tensile specimens were machined to the final shape directly from the casting, while the other samples (to be tested in heat-treated condition) were machined to the final size only after heat treatment in order to ensure the proper dimensional features. The size of tensile specimens was chosen according to UNI EN ISO 6892-1 standard (sample diameter of 5 mm and gauge length of 25 mm).

T6 heat treatments were performed in laboratory furnaces. Solution temperature was chosen according to previous studies on the same alloy (Ref 34) and criteria commonly applied for Al-Si-Mg alloys (Ref 9). In detail, this treatment was carried out for 8 h at 545 °C and subsequently water quenching was performed at 65 °C to guarantee proper cooling conditions (Ref 9). When necessary, specimens were stored at − 20 °C to prevent any natural aging and finally samples were aged at two different temperatures (165 and 190 °C) for various durations.

Aging treatment was performed for 1, 2, 4, 6 and 8 h on samples for microhardness measurements, while for room-temperature tensile tests only three aged conditions were selected (1, 4, and 8 h) according to the obtained hardness aging curves. After data evaluation, tensile tests were performed at high temperatures on samples in one selected aged condition.

In order to carry out the microstructural characterization, samples were observed by optical microscope Leica DMI 5000 M and scanning electron microscope (SEM) LEO EVO 40 equipped with an energy-dispersive spectroscopy (EDS) detector for microanalysis. Samples were ground and polished up to mirror finishing, starting with emery papers (from P220 to 2500 grade) and then using diamond suspensions (grain size of 3 and 1 μm) on velvet cloths. Subsequently, the specimens were cleaned in an ultrasonic bath in ethanol and dried with warm air. Average secondary dendrite arm spacing (SDAS) was calculated according to the linear intercept method. Grain size measurements were taken after electrochemical etching for 90 s in a 4% HBF_4 solution. Samples were observed under polarized light, and the intercept method according to ASTM E112 standard was applied.

Regarding mechanical characterization, first, Vickers microhardness was measured on samples in as-cast, quenched and aged condition by means of a Shimadzu tester (load of 200 g applied for 15 s). Twenty measurements were taken for each sample, and average values and standard deviations were calculated.

The tensile tests at room temperature were performed using Instron 3369 testing machine with a load cell of 50 kN. The

tests were carried out in displacement control mode. During the tests, in the elastic field, the speed of the crosshead was set to 1 mm/min, while it was set to 2 mm/min in the plastic field. An external extensometer with a gauge length of 25 mm was used during testing to get exact elongation values. Three samples were tested for each condition.

High-temperature tensile tests were performed on specimens in a selected aged condition (i.e., 4 h at 165 °C) at 150, 200, 250, 300 °C. The heating and soaking time before testing were kept in the range 40-60 min. Different geometries of the samples and testing procedures were applied for high-temperature test as compared with room-temperature test, according to the different standard. Specimens for high-temperature tests were machined from the central part of the casting with circular cross section and collars, in accordance with UNI EN ISO 6892-2 specifications. In particular, they were characterized by a gauge length of 30 mm and a gauge diameter of 6 mm. Tensile tests were performed in displacement control mode, with a crosshead displacement rate of 1 mm/min. Under these conditions, at the yield point most of the tests were within the strain rate range R2 (nominal strain rate 0.00025 1/s, ± 25%) of the above-mentioned standard.

Due to the significant differences in ductility for the studied alloy according to the test conditions, strain-hardening exponents were calculated with a modified procedure. In fact, in the present paper, strain-hardening exponents were obtained by fitting with a power-law equation a fixed region of the experimental true plastic stress–true plastic strain curves. In particular, the interpolation was carried out from yield strain to the plastic strain corresponding to the maximum applied load (therefore before necking of tensile specimens) for high-temperature tests and from yield strain to the plastic strain at failure for room-temperature tests.

After tensile test, microhardness measurements were taken on the head of tensile specimens, on a cross section close to the gauge length, to identify overaging phenomena due to the exposure to testing temperature. These samples were also observed performing SEM analysis with a Hitachi SU-70 microscope provided with a field emission Schottky electron source and a scanning transmission electron microscope (STEM) detector. These analyses allowed the evaluation of the presence of Cr-containing dispersoids and their evolution during testing at high temperature in comparison with samples in T6 condition, which was also analyzed by STEM with an acceleration voltage of 30 kV. Disks with 3 mm diameter and approximately 100 μm thickness were obtained via mechanical polishing and then electrochemically etched by a double jet commercial instrument. In particular, an acid solution (33% HNO_3 in methanol) was used at − 25 °C with an applied tension of about 15 V.

Finally, fracture surfaces were observed by SEM and cross sections of tested specimens were mirror-polished and analyzed by optical microscope in order to study the fracture mechanism.

3. Results and Discussion

3.1 Microstructural Characterization

AlSi3Cr samples exhibit a dendritic microstructure with the Al matrix surrounded by the eutectic phase (Fig. 1). Average SDAS of 43 ± 5 μm and average grain size of 204 ± 11 μm were measured.

SEM observations allowed the identification of an intermetallic phase with complex morphology containing Fe, Cr and Mn (Fig. 2), indicated as α-Al(Fe,Mn,Cr)Si phase. In fact, the composition (wt.%) at point 1 marker was Al (59.85%), Si (12.38%), Cr (12.59%), Mn (4.33%) and Fe (10.85%), as recorded by EDS measurement. The presence of this phase is due to the addition of Cr and Mn, which are responsible for the variation in the morphology of Fe-based intermetallics, as widely discussed in scientific literature (Ref 35, 36). It is also known that this phase is not strongly affected by heat treatment (Ref 36) and, therefore, SEM analysis in Fig. 2 are presented only for the as-cast condition.

Furthermore, images at higher magnifications (Fig. 3) pointed out also the presence of dispersoids in samples in aged condition (solution at 545 °C for 8 h and aging at 165 °C for 4 h). They appear as incoherent nano-metric particles with a polygonal morphology. The presence of Cr was documented in (Ref 22) for the same alloy. As described in a previous work by the authors (Ref 23), it was observed by means of x-ray absorption spectroscopy (XAS) that these particles form between 400 and 500 °C during heating at 10 °C/min up to solution treatment temperature, while no significant evolution can be detected for prolonged holding time and during aging

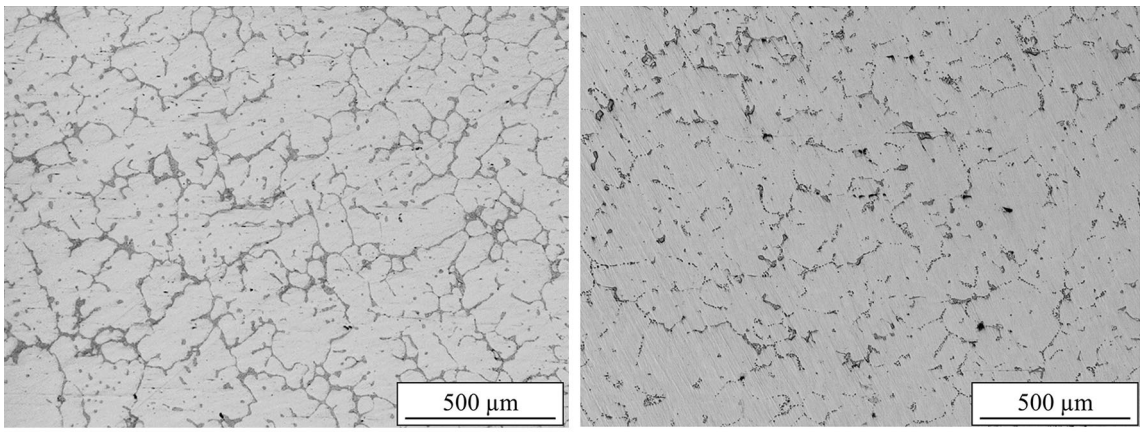

Fig. 1 Micrographs of the studied alloy: (a) as-cast and (b) aged sample (solution treatment at 545 °C for 8 h followed by aging at 165 °C for 4 h)

treatment. This was also confirmed by previous analyses by differential scanning calorimetry (DSC) (Ref 22). Furthermore, XAS analysis (Ref 23) allowed the identification of the crystal structure of dispersoids as face-centered cubic phase with unit cell of 1.09 nm.

From analyses at higher magnification (Fig. 3b), it was possible to observe the pattern of Mg_2Si hardening precipitates, homogeneously distributed in the matrix.

3.2 Vickers Microhardness

Hardness aging curves (Fig. 4) were first used to characterize the samples and to verify the effectiveness of the heat treatment.

The material shows an initial hardness of 73 ± 3 HV in as-cast condition, while the overall material hardness in aged condition ranges between 110 and 130 HV, which represents a significant improvement compared to the as-cast alloy or to the traditional AlSi7 Mg alloy (Ref 9, 16).

The results show that aging time of 8 h is not enough to reach overaging when the aging treatment is performed at 165 °C. In this condition, the material hardness reaches the value of approximately 130 HV. Aging treatment at 190 °C leads to earlier reaching of the peak condition, after only 1 h. It means that also overaging occurs earlier, as shown by the measured data.

For the following mechanical characterization, aging times of 1, 4 and 8 h were selected for both the considered temperatures (165 and 190 °C) as more representative of the response of the material to the aging treatment. In detail, after 1-h aging, it can be observed that the alloy treated at 190 °C reaches the highest values of hardness, while after 8 h the maximum hardness was measured for aging at 165 °C. Based on this, also an intermediate aging time of 4 h was selected. In this condition, the material exhibited the same hardness value for both the investigated aging temperatures, even though for the lower temperature (165 °C) the material is in underaged condition, while for the highest temperature (190 °C) the material is already overaged. It is believed interesting to evaluate if this behavior can be confirmed also in terms of tensile properties, besides in terms of hardness values. In addition, the as-quenched condition was tested in order to have a complete overview of the evolution of mechanical performance of AlSi3Cr alloy since the dispersoids have already formed during this stage.

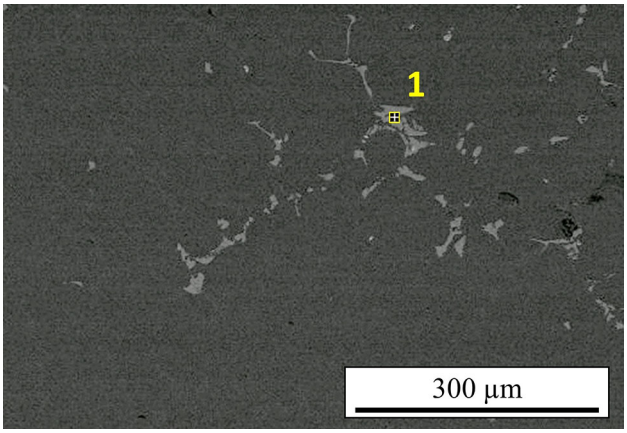

Fig. 2 Image from SEM analysis of intermetallic particles

3.3 Tensile Properties at Room Temperature

The average ultimate tensile strength (UTS), yield strength (YS), elongation (El%) and quality index (QI) of the studied alloy were 204 ± 2, 104 ± 2 MPa, 5.6 ± 0.5% and 316, respectively. The QI, frequently used in foundry, was calculated as indicated by Drouzy et al. (Ref 37, 38):

$$\mathrm{QI} = \mathrm{UTS} + d\log(\mathrm{El}\%)$$

where d is a material constant (150 MPa in the original work; the same value was used also in the present work).

The mechanical properties for the heat-treated samples are reported in Fig. 5. For aging at 165 °C, the peak value of UTS is reached after 4 h aging and the strength remains quite constant for prolonged holding at this temperature. These are the highest values among all the tested conditions. The results for aging treatment performed at 190 °C show that after 1 h of aging treatment no further relevant increase in ultimate strength is measured, but the values rather show a tendency to decrease. Yield strength increases with longer aging time for samples aged at 165 °C, while it is quite constant for aging temperature

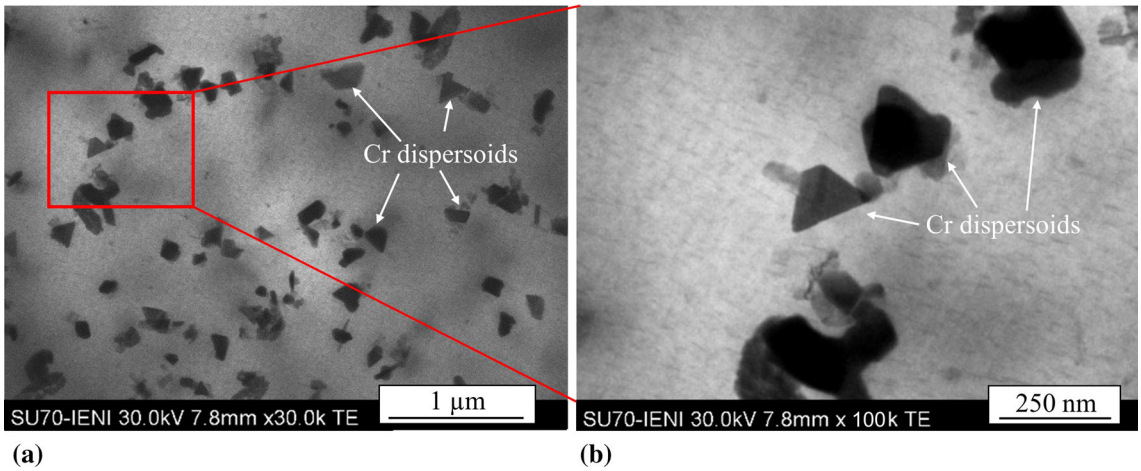

Fig. 3 STEM images of dispersoids containing Cr after T6 treatment (solution treatment at 545 °C for 8 h followed by aging at 165 °C for 4 h) at (a) lower and (b) higher magnification

of 190 °C, even though the differences between the two different aging temperatures are less marked than for UTS. More evident is their effect on the elongation of the material. In fact, aging at 190 °C leads to an abrupt decrease in elongation already after 1 h aging, with values around 2% for all aged conditions. On the other hand, aging at 165 °C allows elongation values of about 6% after 1 h treatment and 4% after 4 h. Longer aging of 8 h results in elongation comparable to the case of aging at 190 °C. The general evolution of tensile properties is similar to what reported in a previous work (Ref 24), where solution treatment was carried out for a shorter duration. After an optimization of solution treatment parameters, in the present study it was possible to reach higher UTS values for aging treatment performed at 165 °C.

QI values in Fig. 5(d) provide an evident comparison of material performance after aging treatment at different temperatures. It appears immediately that aging at 190 °C is not adequate to enhance material properties, while the temperature of 165 °C combined with short treatment time allows to reach highest values of QI, which are reasonable for casting alloys (Ref 39, 40).

Based on experimental results, it was chosen to perform tensile tests at higher temperatures after aging at 165 °C for 4 h as the best compromise between strength and elongation.

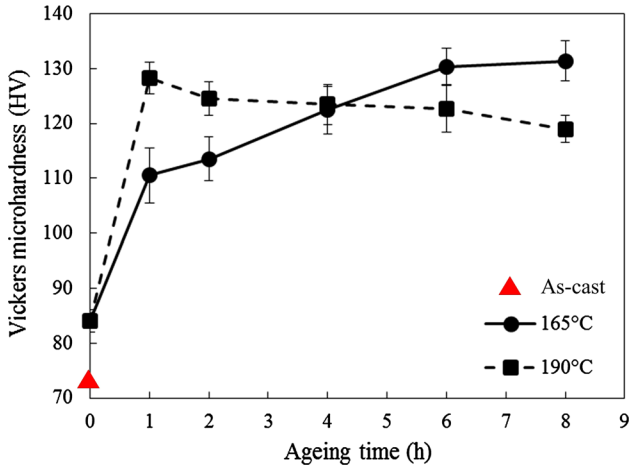

Fig. 4 Hardness aging curves as a function of aging time and temperature

3.4 Tensile Properties at High Temperatures

Tensile properties of the studied alloy in a selected T6 condition (i.e., solution treatment at 545 °C for 8 h followed by aging at 165 °C for 4 h) are shown in Fig. 6 as a function of temperature up to 300 °C. It is evident that the material strength decreases with increasing temperature (Fig. 6a). Despite this tendency, tensile properties at 150 and 200 °C are quite similar (differences of approximately 10%). In this temperature range, the material still exhibits remarkable UTS (in the range 250-275 MPa) and YS (in the range 245-265 MPa), with good elongation (approximately 5%).

A more evident decrease in tensile properties was measured during testing at 250 °C: material strength is reduced of 50% in comparison with room-temperature condition, while the influence of testing temperature on the ductility is limited (elongation of 6%). Finally, at 300 °C the material behavior is characterized by poor strength and high elongation, suggesting

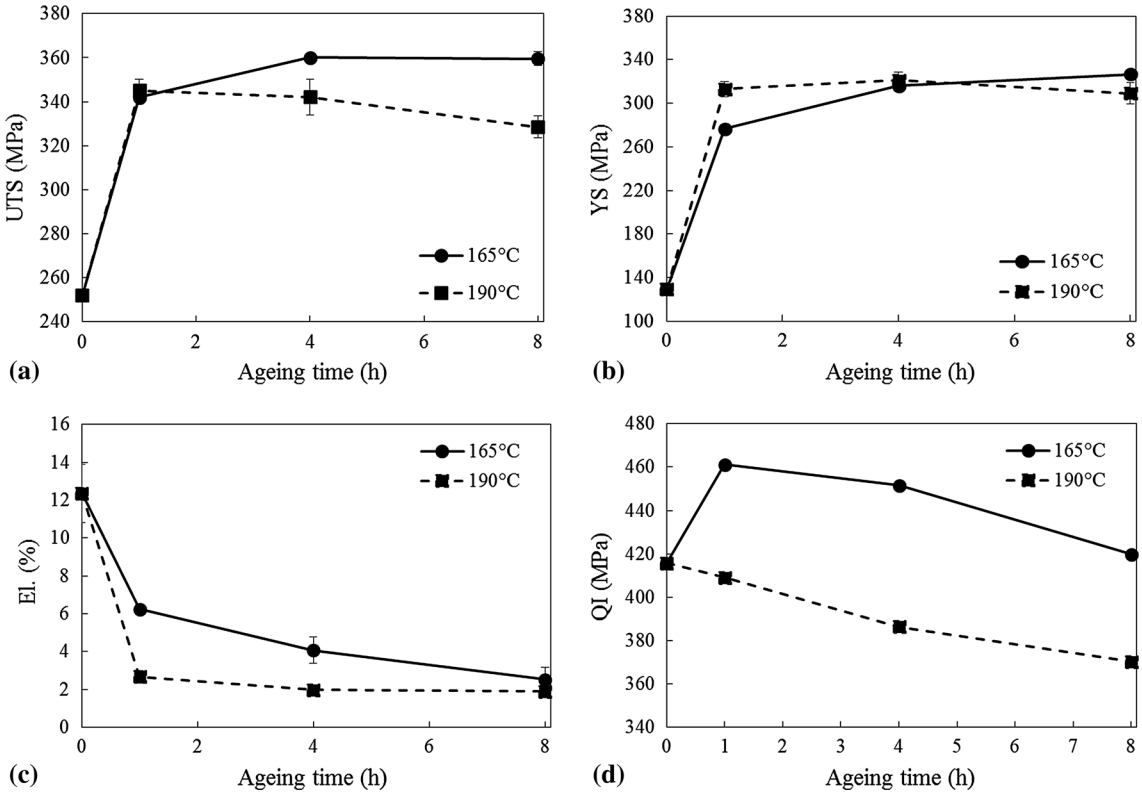

Fig. 5 Aging curves for (a) UTS, (b) YS, (c) elongation and (d) quality index (QI) from tensile tests performed at room temperature on specimens aged at 165 °C and 190 °C

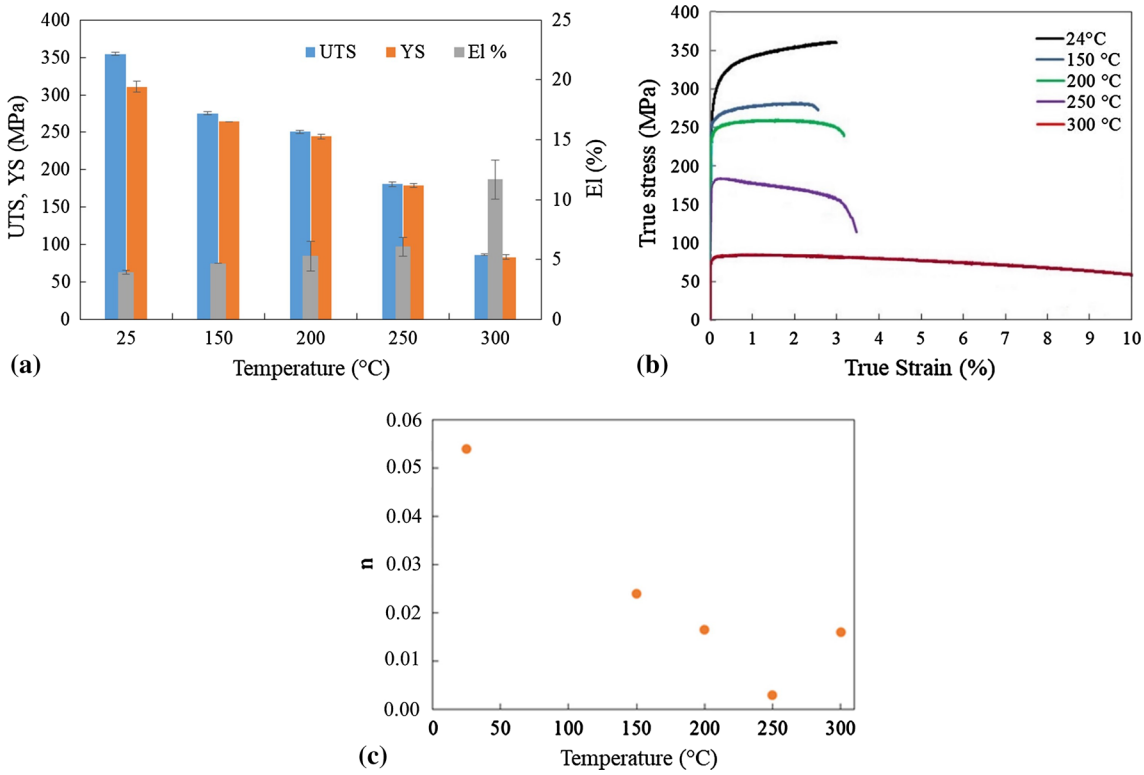

Fig. 6 (a) Tensile properties of the studied alloy in T6 condition (solution treatment at 545 °C for 8 h followed by aging at 165 °C for 4 h), (b) corresponding true stress–true strain curves, (c) straining index n at different test temperatures

a strong effect of temperature on material microstructure and softening of the Al matrix.

Figure 6(b) illustrates the true stress–true plastic strain curves from different experimental tests. The strain-hardening indexes *n*, plotted as a function of temperature in Fig. 6(c), were calculated from curves in Fig. 6(b).

Figure 6(b) shows that the plastic strain at peak stress tends to decrease as the test temperature increases, at least up to 250 °C. This behavior had been previously observed in cast alloys progressively overaged, as it can be considered the case of the present alloy tested at increasingly higher temperatures in T6 condition (Ref 41). Figure 6(c) clearly shows that *n* values decrease as test temperature increases, reaching the minimum value for 250 °C. Further increase in temperature leads *n* to increase. It is well known that strain-hardening index in age-hardening Al alloys is correlated with the actual temper condition, being higher in the as-cast and lower in the solution-treated and peak-aged condition (Ref 42). The strain-hardening values at room temperature obtained in the present investigation are a bit lower than the 0.08-0.17 range reviewed by Elhadari et al. (Ref 43) for A356 alloy in T6 or similar tempers, but are well in agreement with data for A357 alloy in the peak strength conditions reported by Alexopoulos and Tiryakioğlu (Ref 41).

The reduction of strain-hardening index as temperature increases is typical for most materials, but in age-hardened conditions it can combine with strengthening particle precipitation, coarsening, and dissolution occurring as test temperature increases. These phenomena, according to which is dominant in the considered temperature range, can either contribute to the *n*-reduction induced by temperature [such as in the case of as-cast Al-Si-Cu alloys reported in (Ref 44)] or lead to the opposite trend, a strain-hardening index increase with temperature. In this regard, a behavior of *n*-index similar to that shown in Fig. 6(c) was reported by Ferguson et al. (Ref 45), for the Al-Mg-Cu-Si A319 alloy, in a study about the effect of different heat treatments on the *n*-temperature correlation. In addition, the early necking of the sample occurring during test at 300 °C, which strongly reduced the range of strain for the calculation of the strain index, could contribute to the increase in the calculated *n* value.

The average hardness values after exposure to high temperatures during tensile tests were 136 ± 11 HV (150 °C), 143 ± 4 HV (200 °C), 90 ± 4 HV (250 °C) and 75 ± 3 HV (300 °C), respectively. As indicated by the previously reported aging curves (Fig. 4), the material was not tested in peak-aged condition in terms of hardness. For this reason, a further exposure to temperatures close to the aging one led to an increase in material hardness due to the formation of an additional amount of β′-Mg_2Si precipitates. On the other hand, after holding at temperatures of 250 and 300 °C, the material suffered from overaging likely due to the coarsening and dissolution of the Mg-containing particles, resulting in a severe loss in hardness.

In order to better explain these findings and their correlation to the microstructural evolution after exposure at high temperatures during tensile tests, samples taken from specimens tested at 200 and 300 °C were observed by STEM. These two samples were selected in order to compare a condition in which the material still retains most of its initial strength (200 °C) with a condition where the material resistance is significantly reduced (300 °C).

Images in Fig. 7 clearly show a significant coarsening of Mg_2Si particles after exposure to 300 °C, which can be easily identified as small rods in Fig. 7(b), while this is not possible in

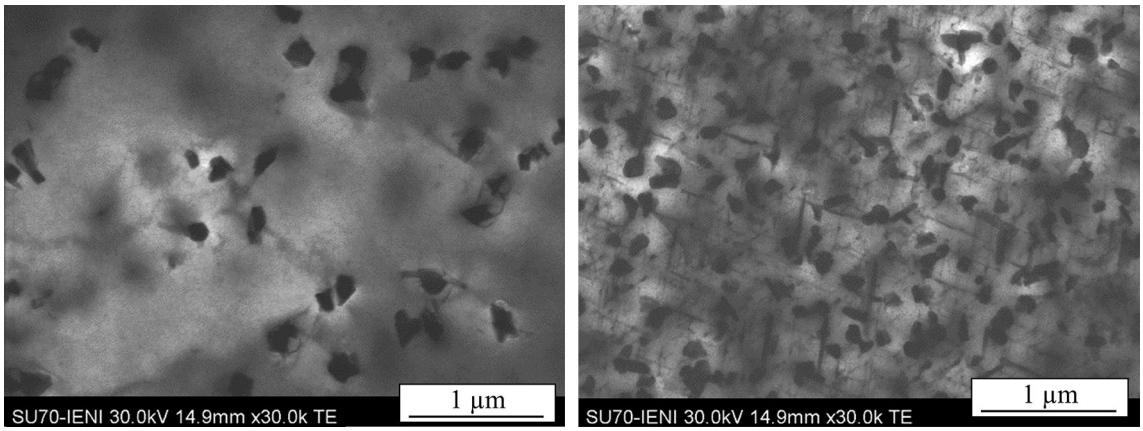

Fig. 7 STEM images after tensile test at (a) 200 °C and (b) 300 °C (non-deformed area)

Fig. 7(a) due to their lower size and (semi-)coherence with the Al matrix. The formation of incoherent Mg_2Si particles leads to the loss of their strengthening effect. Furthermore, an increase in the number of dispersoids can be appreciated, which appear more uniformly distributed in the Al matrix. The identification of dispersoids is supported by previous studies on the same alloy based on EDS (Ref 22) and XAS (Ref 23) analysis. As previously mentioned, the latter revealed also the crystal structure of dispersoids, as face-centered cubic phase with unit cell of 1.09 nm.

The differences in the features of intragranular particles in the alloy strained at 200 and 300 °C could contribute to the increase in strain-hardening exponent at 300 °C (Fig. 6c), combined with the coarsening of Mg_2Si, as reported also by Ferguson et al. (Ref 45). Furthermore, it is also consistent with the alloy softening at 300 °C and with the greater elongation at rupture experienced by the specimen tested at 300 °C.

The formation of additional dispersoids is also interesting since it is reported for the studied alloy that these particles nucleate during heating between 400 and 500 °C when the heating rate is 10 °C/min (Ref 23). Nevertheless, it should be considered that the formation of dispersoids is highly affected by the heating rate and by the formation of Mg-Si phases as precursors, as reported by various studies (Ref 46, 47). In particular, according to different authors (Ref 46, 47), the slower the heating rate, the more uniform the distribution of dispersoids. For tensile test at 300 °C, a heating rate below 10 °C/min can be estimated. Therefore, this factor should be taken into account to understand the additional precipitation of Cr-containing particles observed in Fig. 7(b) after exposure to 300 °C.

Furthermore, Lodgaard and Ryum (Ref 46, 48) proposed a model for the precipitation of dispersoids where, as above mentioned, Mg-Si phases behave as precursors. According to their analysis on various Al-Mg-Si wrought alloys (6000 series), dispersoids form through Mn/Cr and Fe diffusion into the precursor β′-Mg_2Si phase. The dispersoids precipitate along an intermediate phase, called 'u-phase' (Ref 46). If the material is in as-cast condition, during heat treatment, first the precipitation of the precursor β′-Mg_2Si phase takes place, then they allow the formation of dispersoids. In the considered case, the material is heated up to 300 °C in T6 condition. It means that the precursor β′-Mg_2Si phase is already present in the Al matrix. Consequently, the presence of this precursor phases in the material, which was already in T6 condition, could have enhanced the formation of dispersoids during heating up to 300 °C, as observed in Fig. 7(b).

Moreover, not only the temperature, but also the soaking time is an important parameter to consider. In this regard, the precipitation of dispersoids could be enhanced also by the fact that the alloy was held in isothermal condition for a certain time. This is in agreement with a recent study by Kemsies et al. (Ref 49) where an adapted heat treatment tailored to enhance the precipitation of fine Mn-containing dispersoids was proposed by decreasing the conventional treatment temperature and selecting a proper soaking time.

Therefore, it is believed that applying a heating rate below 10 °C/min up to 300 °C to the material in T6 condition and holding it at this temperature during tensile testing provided enough energy to the material to allow diffusion phenomena and the formation of additional dispersoids, despite the lower temperature in comparison with the solution treatment. It follows that the formation of additional dispersoids would take place in case of exposure to similar temperature in service.

On the other hand, no evident coarsening of dispersoids is observed, confirming that, once formed, they are thermally stable at the considered temperature.

This microstructural evolution is not sufficient to avoid a decrease in strength due to the general softening of the Al matrix and the presence of creep effects, which lead to lower strength and higher elongation at 300 °C in comparison with room-temperature condition. Material deformation mechanisms are strongly affected by temperature. In this regard, the movement of dislocation is accelerated by increased temperature, since they are able to bypass obstacle by climbing, together with an increase in the number of activated slip planes. In addition, the coarsening of Mg-Si precipitates is negative for material strength since they are less effective in hindering dislocation motion. It is well known that when β-Mg_2Si precipitates lose their coherency with the matrix, they are less able in pinning deformation (Ref 50).

In order to evaluate the possibility to use the studied alloy for high-temperature applications, as the main aim of the present study, a comparison with the performances of alloys with similar composition and/or for equivalent applications is helpful. In Table 1, tensile properties at room temperature and 200 °C of these alloys are summarized.

Table 1 Comparison of tensile properties at room temperature and 200 °C for different Al-Si-Mg alloys

Alloy	SDAS, µm	*T*, °C	UTS, MPa	YS, MPa	El, %	Ref.
AlSi3Cr	43 ± 5	25	355	311	4	Present study
		200	251	244	5.3	Present study
C355 (Al-Si-Cu-Mg)	66 ± 5	25	327	287	4.3	6
		200	237	221	8.5	
C355 (Al-Si-Cu-Mg)	20 ± 2	25	361	293	10	6
		200	248	232	11.7	
A356	32 ± 3	25	248	213	1.3	20
		200	177	169	2.1	
A356 + 0.3 wt.% Er	24 ± 1	25	280	255	4.5	20
		200	220	215	5.5	
A356 + 0.3 wt.% Er + 0.5 wt.% Zr	18 ± 1	25	290	270	4.5	19
		200	260	240	4.5	
Al-Si-Cu-Mg + Ti,V,Zr,Cr	25	25	320	300	2.5	12
		200	240	230	2	
AlSi7Cu2 Mg + 0.2 wt.% Zr	…	25	335	291	2	51
		200	246	224	4	

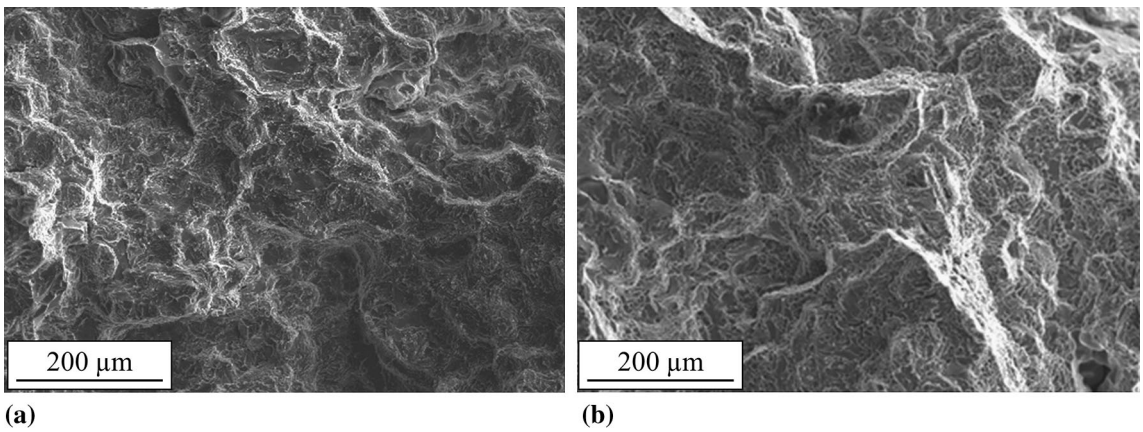

Fig. 8 Surface fracture of tensile samples in (a) as-cast and (b) aged condition

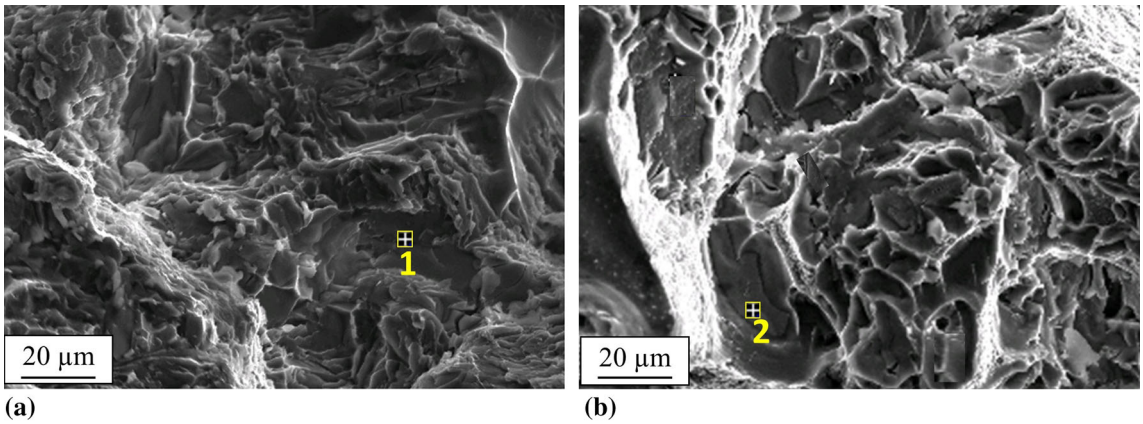

	Al	Si	Cr	Mn	Fe
1	58.81	13.83	12.23	3.82	11.31
2	79.53	11.82	3.44	1.13	4.08

Fig. 9 Detail of the fracture surfaces for specimens tested in (a) as-cast, (b) aged condition and corresponding EDS analysis (wt.%)

It is interesting to observe that the performance of AlSi3Cr alloy at high temperature is comparable with those of AlSi7 Mg alloys modified with different alloying elements, as such as Ti, V and Zr, together with Cr (Ref 12), or Er and Zr (Ref 19), added to improve the high-temperature properties. Regarding the properties at 200 °C, the studied alloy exhibits higher YS and similar UTS. In comparison with the alloy containing Cr-Ti-V-Zr, AlSi3Cr alloy reaches higher elongation, which is a key parameter for the design of certain structural components. Furthermore, the addition of V, Zr or Er represents a quite expensive solution, which can make the choice of the studied alloy more affordable and easier to manage for industrial production. On the other hand, AlSi3Cr alloy exhibits lower elongation as compared to C355 alloy (Ref 6), but the addition of Cr, instead of Cu, can represent a positive aspect for corrosion resistance.

In general, the mentioned alloys displayed microstructural features very similar to the studied AlSi3Cr alloy, as such as the presence of intermetallic particles with a complex morphology, the formation of dispersoids during heat treatment, similar Mg

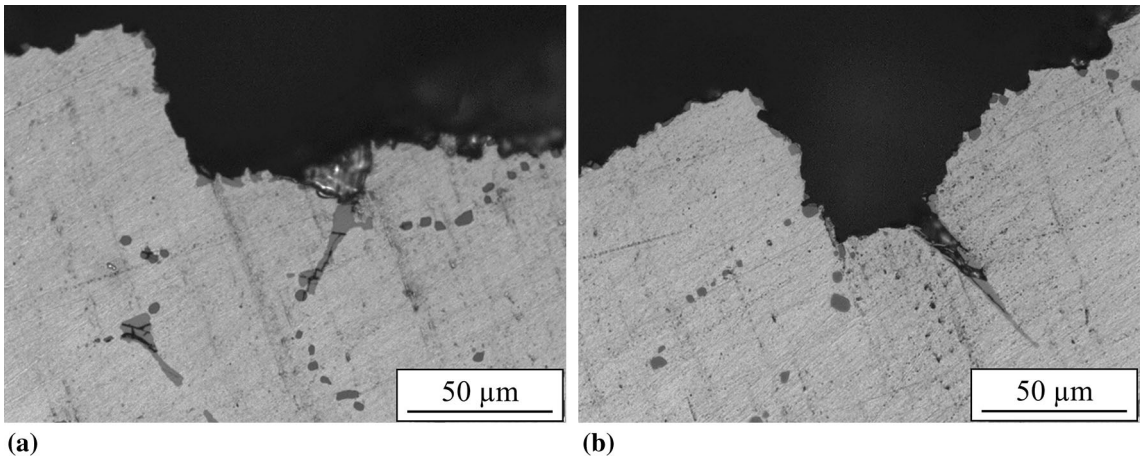

Fig. 10 (a, b) Cross section of fractured tensile specimen in aged condition (solution treatment at 545 °C for 8 h followed by aging at 165 °C for 4 h) where cracked intermetallic particles are visible

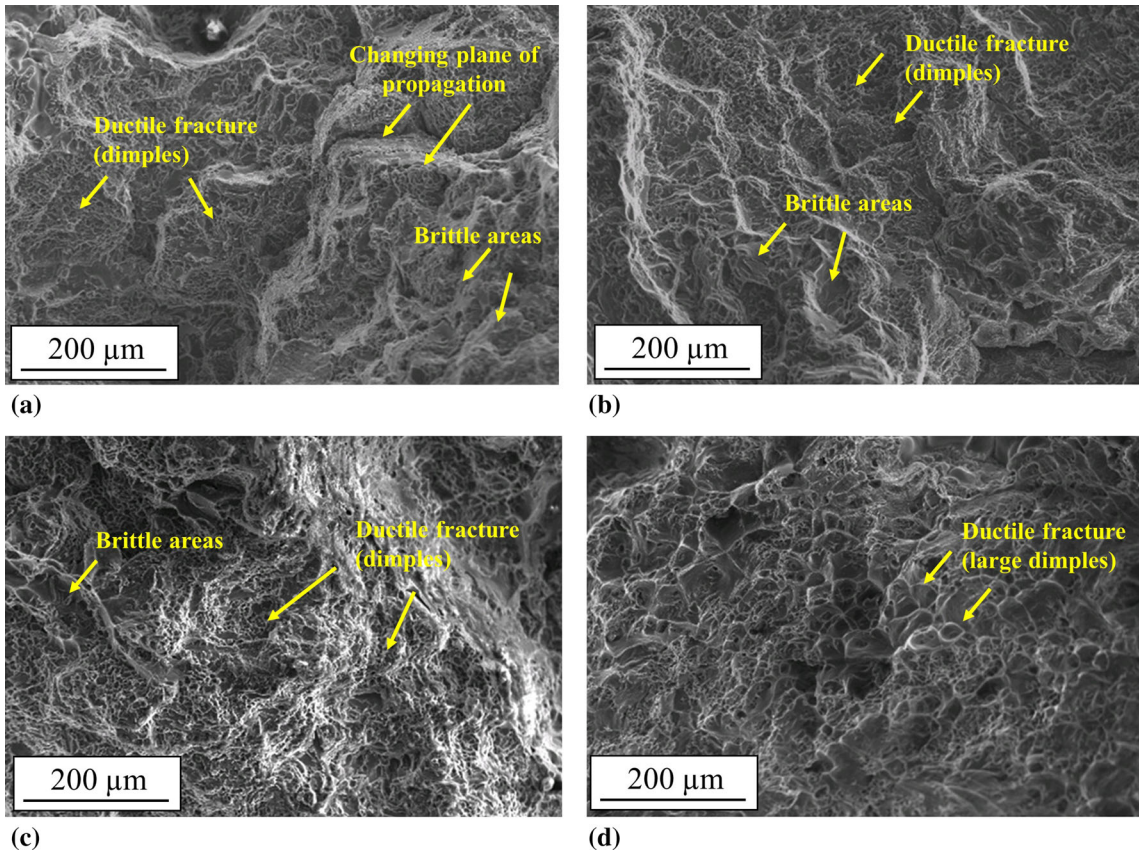

Fig. 11 SEM images of fracture surfaces of after tensile test at (a) 150 °C, (b) 200 °C, (c) 250 °C, (d) 300 °C

content. A significant different feature is represented by the reduced Si content of the AlSi3Cr alloy, which corresponds to 13% of eutectic phase in comparison with 49% for AlSi7 alloys.

In this regard, as previously mentioned, Si content is reported to significantly affect mechanical properties of Al-Si alloys, enhancing material hardness and strength, but reducing ductility (Ref 26-28). Nevertheless, the obtained results show that AlSi3Cr alloy exhibits similar or even improved tensile strength at high temperature than alloys with higher Si content. It follows that a lower Si content in comparison with more conventional compositions is not to be considered as a critical aspect for tensile strength at high temperatures, if the Al matrix is properly strengthened. This can represent an interesting additional way to improve material performance by optimization of chemical composition, besides the addition of strengthening elements.

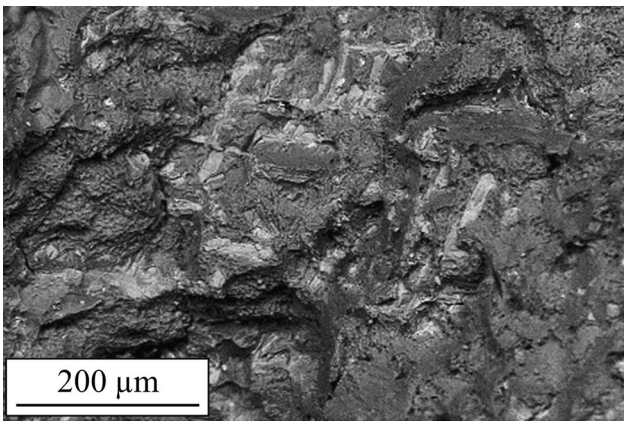

Fig. 12 Detail of intermetallic particles emerging on the fracture surface

Furthermore, based on data on thermal expansion coefficient from (Ref 52) and dilatometry test on similar alloys (Ref 53, 54), it is believed that the considered Si content is not critical for dimensional stability at high temperature, given also the study for high-temperature application of alloys with only slightly higher concentration of Si (319 alloy with 5-6% and A356 alloy with 7% Si).

Finally, further improvement in fracture elongation can be obtained by refining the material microstructure (Ref 6), since the measured SDAS and grain size are quite coarse. This suggests that AlSi3Cr alloy could reach even more remarkable performance, allowing a reduction of thickness of components and therefore contributing to reducing the overall weight of vehicles, ensuring at the same time high mechanical properties at high temperature.

3.5 Analysis of Fracture Surfaces

The fracture surfaces of samples tested at room temperature in as-cast and aged condition exhibit a mainly ductile fracture mechanism with small micro-deformations (dimples), as detectable in Fig. 8. Despite that some cracked intermetallic particles were identified on the surface (Fig. 9 and 10), the overall failure mechanism mainly follows the eutectic path, as easily detectable from the analysis of the cross sections of the fractured samples.

Regarding tensile tests at high temperatures, images in Fig. 11 show an evolution toward a more ductile morphology

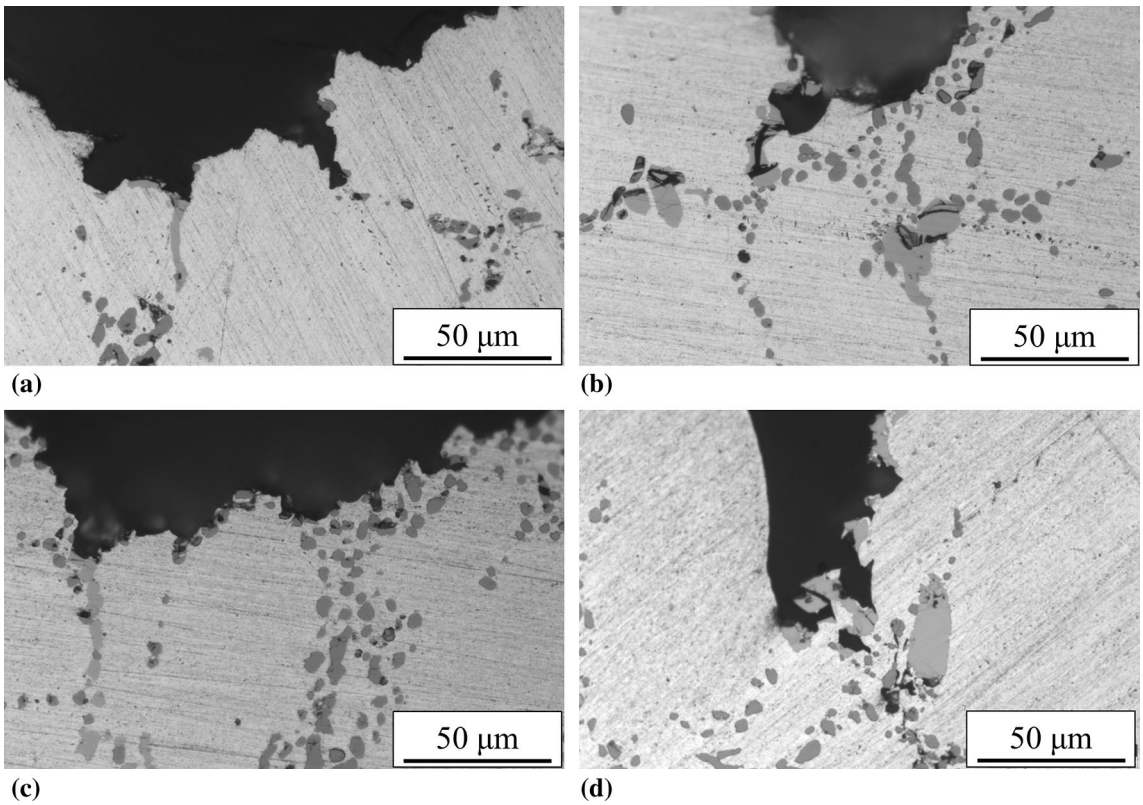

Fig. 13 Cross section of fractured tensile specimen after tensile test at (a) 150 °C, (b) 200 °C, (c) 250 °C, (d) 300 °C

with increasing the testing temperature. This is particularly evident for the sample tested at 300 °C (Fig. 11d) where larger dimples than in samples tested at lower temperature are visible.

In some areas, clusters of intermetallic particles emerge on the fracture surface. An example is noticeable in the SEM image acquired in back-scattered mode (Fig. 12) for the samples tested at 200 °C. These may be responsible for the abrupt changes in the plane of fracture propagation. Such cracked particles were present on all samples tested, as visible from the observation of the cross section of fractured specimens (Fig. 13). Also Si particles are present, as expected since it was observed that the fracture mainly follows the eutectic phase.

4. Conclusions

The present work aimed at evaluating the tensile properties of AlSi3Cr alloy at high temperature. It was found that the studied material exhibits remarkable properties at 200 °C, comparable or higher than those reported in the literature for Al-Si-Mg casting alloys modified with Cu, Zr, Er and other transition metals/rare earth elements. The aluminum matrix of the studied alloy is strengthened by Cr-containing dispersoids that are thermally stable at this temperature, as demonstrated by STEM images, and enhance tensile properties up to 200 °C. At higher temperatures, alloy resistance decreases for a general softening of the material. Interestingly, it was found that at 300 °C dispersoids do not dissolve but rather increase in number. The additional precipitation of dispersoids provides an unexpected indication for new heat treatments routes that can enhance their uniform distribution in the Al matrix in order to further promote material properties. Finally, the reduced Si content in comparison with conventional cast alloys appears not to be negative for microstructural and mechanical properties, suggesting an alternative way to design high-resistance alloys.

Acknowledgments

The authors would like to thank Maxion Wheels Italia Srl for providing the alloy, F. Peli (Dept. of Mechanical and Industrial Engineering of the University of Brescia) for his support in tensile samples preparation and Dr. L. Montesano (Dept. of Mechanical and Industrial Engineering of the University of Brescia) for SEM analysis.

References

1. Mahle GmbH, Ed., *Pistons and Engine Testing*, Springer Science & Business Media, Stuttgart, 2012, p 59–76
2. J. Man, L. Jing, and S. Jie, The Effects of Cu Addition on the Microstructure and Thermal Stability of an Al-Mg-Si Alloy, *J. Alloys Compd.*, 2007, **437**, p 146–150
3. M. Zamani, S. Seifeddine, and A. Jarfors, High Temperature Tensile Deformation Behavior and Failure Mechanisms of an Al-Si-Cu-Mg Cast Alloy—The Microstructural Scale Effect, *Mater. Des.*, 2015, **86**, p 361–370
4. Y. Li, S. Brusethaug, and A. Olsen, Influence of Cu on the Mechanical Properties and Precipitation Behavior of AlSi7Mg0.5 Alloy During Aging Treatment, *Scr. Mater.*, 2006, **54**, p 99–103
5. M. Javidani and D. Larouche, Application of Cast Al-Si Alloys in Internal Combustion Engine Components, *Int. Mater. Rev.*, 2014, **59**(3), p 132–158
6. L. Ceschini, A. Morri, A. Morri, S. Toschi, S. Johansson, and S. Seifeddine, Effect of Microstructure and Overaging on the Tensile Behavior at Room and Elevated Temperature of C355-T6 Cast Aluminum Alloy, *Mater. Des.*, 2015, **83**, p 626–634
7. E. Kilinc and Y. Birol, Optimising the T6 Heat Treatment for Gravity Cast AlSi7MgCu0.5 Alloy V8 Cylinder Heads, *Int. J. Cast Met. Res.*, 2017, **30**(4), p 244–250
8. S. Roy, L. Allard, A. Rodriguez, T. Watkins, and A. Shyam, Comparative Evaluation of Cast Aluminum Alloys for Automotive Cylinder Heads: Part I—Microstructure Evolution, *Metall. Mater. Trans. A*, 2017, **48**(5), p 2529–2542
9. J.R. Davis, Ed., *ASM Speciality Handbook, Aluminum and Aluminum Alloys*, ASM International, Davis & Associates, Materials Park, 1993
10. W. Kasprzak, B. Amirkhiz, and M. Niewczas, Structure and Properties of Cast Al-Si Based Alloy with Zr-V-Ti Additions and Its Evaluation of High Temperature Performance, *J. Alloys Compd.*, 2014, **595**, p 67–79
11. S. Shaha, F. Czerwinski, W. Kasprzak, J. Friedman, and D. Chen, Improving High-Temperature Tensile and Low-Cycle Fatigue Behavior of Al-Si-Cu-Mg Alloys Through Micro-additions of Ti, V, and Zr, *Metall. Mater. Trans. A*, 2015, **46A**, p 3063–3078
12. S. Shaha, F. Czerwinski, W. Kasprzak, J. Friedman, and D. Chen, Ageing Characteristics and High-Temperature Tensile Properties of Al-Si-Cu-Mg Alloys with Micro-Additions of Cr, Ti, V and Zr, *Mater. Sci. Eng. A*, 2016, **652**, p 353–364
13. M. Zamani, L. Morini, L. Ceschini, and S. Seifeddine, The Role of Transition Metal Additions on the Ambient and Elevated Temperature Properties of Al-Si Alloys, *Mater. Sci. Eng. A*, 2017, **693**, p 42–50
14. M. Di Giovanni, E. Cerri, D. Casari, M. Merlin, L. Arnberg, and G. Garagnani, The Influence of Ni and V Trace Elements on High-Temperature Tensile Properties and Aging of A356 Aluminum Foundry Alloy, *Metall. Mater. Trans. A*, 2016, **47**(5), p 2049–2057
15. L. Lattanzi, M. Di Giovanni, M. Giovagnoli, A. Fortini, M. Merlin, D. Casari, M. Di Sabatino, E. Cerri, and G. Garagnani, Room Temperature Mechanical Properties of A356 Alloy with Ni Additions from 0.5 to 2 wt.%, *Metals*, 2018, **8**, p 224
16. S. Pramod, A.K.P. Rao, B. Murty, and S. Bakshi, Effect of Sc Addition and T6 Aging Treatment on the Microstructure Modification and Mechanical Properties of A356 Alloy, *Mater. Sci. Eng. A*, 2016, **674**, p 438–450
17. S. Mondol, T. Alam, R. Banerjee, S. Kumar, and K. Chattopadhyay, Development of a High Temperature High Strength Al Alloy by Addition of Small Amounts of Sc and Mg to 2219 Alloy, *Mater. Sci. Eng. A*, 2017, **687**, p 221–231
18. A. Farkoosh, X. Grant Chen, and M. Pekguleryuz, Dispersoid Strengthening of a High Temperature Al-Si-Cu-Mg Alloy via Mo Addition, *Mater. Sci. Eng. A*, 2015, **620**, p 181–189
19. M. Colombo, E. Gariboldi, and A. Morri, Influences of Different Zr Additions on the Microstructure, Room and High Temperature Mechanical Properties of an Al-7Si-0.4 Mg Alloy Modified with 0.25%Er, *Mater. Sci. Eng. A*, 2018, **713**, p 151–160
20. M. Colombo, E. Gariboldi, and A. Morri, Er Addition to Al-Si-Mg-Based Casting Alloy: Effects on Microstructure, Room and High Temperature Mechanical Properties, *J. Alloys Compd.*, 2017, **708**, p 1234–1244
21. Z. Gao, H. Li, Y. Lai, Y. Ou, and D. Li, Effects of Minor Zr and Er on Microstructure and Mechanical Properties of Pure Aluminum, *Mater. Sci. Eng. A*, 2013, **580**, p 92–98
22. M. Tocci, R. Donnini, G. Angella, and A. Pola, Effect of Cr and Mn Addition and Heat Treatment on AlSi3Mg Casting Alloy, *Mater. Charact.*, 2017, **123**, p 75–82
23. M. Tocci, M. Losio, P. Suwanpinji, and A. Pola, Experimental Investigation on the Formation of Cr-Containing Dispersoids in an AlSi3 Alloy by X-Ray Synchrotron Radiation, *J. Alloys Compd.*, 2018, **742**, p 555–562
24. M. Tocci, A. Pola, L. Montesano, G. La Vecchia, M. Merlin, and G. Garagnani, Investigation of Mechanical Properties of AlSi3Cr Alloy, *Frattura Integr. Strutt.*, 2017, **42**, p 337–351
25. G. Gottardi, M. Tocci, M. Montesano, and A. Pola, Cavitation Erosion Behaviour of an Innovative Aluminium Alloy for Hybrid Aluminium Forging, *Wear*, 2018, **394–395**, p 1–10
26. Y. Wang, H. Liao, Y. Wu, and J. Yang, Effect of Si Content on Microstructure and Mechanical Properties of Al-Si-Mg Alloys, *Mater. Des.*, 2014, **53**, p 634–638

27. B. Zhu, P. Leisner, S. Seifeddine, and E. Jarfors, Influence of Si and Cooling Rate on Microstructure and Mechanical Properties of Al-Si-Mg Cast Alloys, *Surf. Interface Anal.*, 2016, **48**, p 861–869
28. D. Dwivedi, R. Sharma, and A. Kumar, Influence of Silicon Content and Heat Treatment Parameters on Mechanical Properties of Cast Al-Si-Mg Alloys, *Int. J. Cast Met. Res.*, 2006, **19**(5), p 275–282
29. S. Joseph and S. Kumar, A Systematic Investigation of Fracture Mechanisms in Al-Si Based Eutectic Alloy-Effect of Si Modification, *Mater. Sci. Eng. A*, 2013, **588**, p 111–124
30. M. Dighe and A. Gokhale, Relationship Between Microstructural Extremum and Fracture Path in a Cast Al-Si-Mg Alloy, *Scr. Mater.*, 1997, **9**(1), p 1435–1440
31. C. Caceres, C. Davidson, and J. Griffiths, The Deformation and Fracture Behaviour of an AlSiMg Casting Alloy, *Mater. Sci. Eng. A*, 1995, **197**(2), p 171–179
32. T. Hosch and R. Napolitano, The Effect of the Flake to Fiber Transition in Silicon Morphology on the Tensile Properties of Al-Si Eutectic Alloys, *Mater. Sci. Eng. A*, 2010, **582**(1), p 226–232
33. A. Fortini, L. Lattanzi, M. Merlin, and G. Garagnani, Comprehensive Evaluation of Modification Level Assessment in Sr-Modified Aluminium Alloys, *Int. J. Metalcast.*, 2018, **12**(4), p 697–711
34. M. Tocci, A. Pola, L. Raza, L. Armellin, and U. Afeltra, Optimization of Heat Treatment Parameters for a Non-conventional Al-Si-Mg Alloy with Cr Addition by DoE Method, *Metall. Ital.*, 2016, **6**, p 141–144
35. S. Shabestari, The Effect of Iron and Manganese on the Formation of Intermetallic Compounds in Aluminum-Silicon Alloys, *Mater. Sci. Eng. A*, 2004, **383**, p 289–298
36. J. Taylor, Iron-Containing Intermetallic Phases in Al-Si Based Casting Alloys, *Procedia Mater. Sci.*, 2012, **1**, p 19–33
37. M. Drouzy, S. Jacob, and M. Richard, Interpretation of Tensile Results by Means of Quality Index and Probable Yield Strength, *AFS Int. Cast Met. J.*, 1980, **5**(2), p 43–50
38. M. Tiryakioğlu, J. Campbell, and N. Alexopoulos, Quality Indices for Aluminum Alloy Castings: A Critical Review, *Metall. Mater. Trans. B*, 2009, **40B**, p 802–811
39. C. Càceres, Microstructure Design and Heat Treatment Selection for Casting Alloys Using the Quality Index, *J. Mater. Eng. Perform.*, 2000, **9**(2), p 215–221
40. C. Càceres, I. Svensson, and J. Taylor, Strength-Ductility Behaviour of Al-Si-Cu-Mg Casting Alloys in T6 Temper, *Int. J. Cast Met. Res.*, 2003, **15**(5), p 531–543
41. N. Alexopoulos and M. Tiryakioğlu, On the Uniform Elongation of Cast Al-7%Si-0.6%Mg (A357) Alloys, *Mater. Sci. Eng. A*, 2009, **507**, p 236–240
42. E. Sjolander, Heat Treatment of Al-Si-Cu-Mg Casting Alloys, Ph.D. Dissertation, Department of Mechanical Engineering School of Engineering, Jönköping University, 2011
43. H. Elhadari, H. Patel, D. Chen, and W. Kasprzak, Tensile and Fatigue Properties of Cast Aluminium Alloy with Ti, Zr and V Additions, *Mater. Sci. Eng. A*, 2011, **528**, p 8128–8138
44. E. Gariboldi, J. Lemke, L. Rovatti, O. Baer, G. Timelli, and F. Bonollo, High Temperature Behavior of High Pressure Die Cast Alloys Based on the Al-Si-Cu System: The Role Played by Chemical Composition, *Metals*, 2018, **8**(5), p 348
45. J. Ferguson, H. Lopez, K. Cho, and C. Kim, Temperature Effects on the Tensile Properties of Precipitation-Hardened Al-Mg-Cu-Si Alloys, *Metals*, 2016, **6**, p 43
46. L. Lodgaard and N. Ryum, Precipitation of Dispersoids Containing Mn and/or Cr in Al-Mg-Si Alloys, *Mater. Sci. Eng. A*, 2000, **283**, p 144–152
47. R. Hu, T. Ogura, H. Tezuka, T. Sato, and Q. Liu, Dispersoid Formation and Recrystallization Behavior in an Al-Mg-Si-Mn Alloy, *J. Mater. Sci. Technol.*, 2010, **26**, p 237
48. L. Lodgaard and N. Ryum, Precipitation of Chromium Containing Dispersoids in Al-Mg-Si Alloys, *Mater. Sci. Technol.*, 2000, **16**, p 599–604
49. R. Kemsies, B. Milkereit, S. Wenner, R. Holmestad, and O. Kessler, In Situ DSC Investigation Into the Kinetics and Microstructure of Dispersoid Formation in Al-Mn-Fe-Si(-Mg) Alloys, *Mater. Des.*, 2018, **146**, p 96–107
50. D. Askeland, P. Fulay, and W. Wright, *The Science and Engineering of Materials*, Cengage Learning, Boston, 2011
51. M. Rahimian, S. Amirkhanlou, P. Blake, and S. Ji, Nanoscale Zr-Containing Precipitates: A Solution for Significant Improvement of High-Temperature Strength in Al-Si-Cu-Mg Alloys, *Mater. Sci. Eng. A*, 2018, **721**, p 328–338
52. P. Hidnert and H. Krider, Thermal Expansion of Aluminum and Some Aluminum Alloys, *J. Res. Natl. Bur. Stand.*, 1952, **48**(3), p 209–220
53. W. Kasprzak, D. Chen, and S. Shaha, Heat Treatment Development for a Rapidly Solidified Heat Resistant Cast Al-Si Alloy, *J. Mater. Eng. Perform.*, 2013, **22**(7), p 1839–1847
54. H. Lopez, Microstructural Features Associated with the Effect of Temperature on the Dimensional Stability of an Automotive Al-A319 Alloy, *AIMS Mater. Sci.*, 2016, **3**(2), p 634–644